Molecular Cell
Article

Single-Cell Analysis Reveals that Noncoding RNAs Contribute to Clonal Heterogeneity by Modulating Transcription Factor Recruitment

Stacie L. Bumgarner,[1,5] Gregor Neuert,[2,5] Benjamin F. Voight,[3,4] Anna Symbor-Nagrabska,[1] Paula Grisafi,[1] Alexander van Oudenaarden,[2,*] and Gerald R. Fink[1,*]
[1]Whitehead Institute for Biomedical Research, 9 Cambridge Center, Cambridge, MA 02142, USA
[2]Department of Physics, Massachusetts Institute of Technology, 77 Massachusetts Avenue, Cambridge, MA 02139, USA
[3]Broad Institute of Harvard and MIT, 7 Cambridge Center, Cambridge, MA 02142, USA
[4]Department of Pharmacology, University of Pennsylvania Perelman School of Medicine, 3400 Civic Center Boulevard, Philadelphia, PA 19104, USA
[5]These authors contributed equally to this work
*Correspondence: avano@mit.edu (A.v.O.), gfink@wi.mit.edu (G.R.F.)
DOI 10.1016/j.molcel.2011.11.029

SUMMARY

Mechanisms through which long intergenic noncoding RNAs (ncRNAs) exert regulatory effects on eukaryotic biological processes remain largely elusive. Most studies of these phenomena rely on methods that measure average behaviors in cell populations, lacking resolution to observe the effects of ncRNA transcription on gene expression in a single cell. Here, we combine quantitative single-molecule RNA FISH experiments with yeast genetics and computational modeling to gain mechanistic insights into the regulation of the *Saccharomyces cerevisiae* protein-coding gene *FLO11* by two intergenic ncRNAs, *ICR1* and *PWR1*. Direct detection of *FLO11* mRNA and these ncRNAs in thousands of individual cells revealed alternative expression states and provides evidence that *ICR1* and *PWR1* contribute to *FLO11*'s variegated transcription, resulting in Flo11-dependent phenotypic heterogeneity in clonal cell populations by modulating recruitment of key transcription factors to the *FLO11* promoter.

INTRODUCTION

Two *cis*-interfering long intergenic ncRNAs, *ICR1* and *PWR1*, regulate transcription of nearby protein-coding gene *FLO11* in the yeast *Saccharomyces cerevisiae* (Bumgarner et al., 2009). These ncRNAs form a bidirectional toggle, one component of a regulatory circuitry that also includes upstream signaling pathways, transcription factors (e.g., activator Flo8 and repressor Sfl1), and chromatin remodelers (e.g., Rpd3L and Hda1 histone deacetylases [HDACs]) (Liu et al., 1996; Rupp et al., 1999; Guo et al., 2000; Pan and Heitman, 2002; Halme et al., 2004; Octavio et al., 2009). In their length, position relative to the *FLO11* coding region, and effects on *FLO11* transcription, *ICR1* and *PWR1* recall phenomena observed at the yeast *SER3* locus (Martens et al., 2004) but are distinct from other types of ncRNA transcription reported at yeast promoters (Seila et al., 2008; Xu et al., 2009; Neil et al., 2009). The ~3.2 kb *ICR1* ncRNA initiates ~3.4 kb upstream of the *FLO11* ORF and represses *FLO11* transcription in *cis*, whereas ~1.2 kb *PWR1* is transcribed from the opposite strand and promotes *FLO11* transcription by interfering in *cis* with *ICR1* (Bumgarner et al., 2009). Competitive binding of *trans*-acting Flo8 or Sfl1 to the *FLO11* promoter (Pan and Heitman, 2002) helps to determine which of the two ncRNAs is transcribed (Bumgarner et al., 2009), resulting in alternative *FLO11* expression states. Rpd3L$^-$ loss-of-function mutants (e.g., *cti6*) exhibit elevated *ICR1* levels, reduced *FLO11* expression, and loss of Flo11-dependent phenotypes similar to a *flo8* null (Bumgarner et al., 2009). Thus, the HDAC Rpd3L appears to be an activator of *FLO11* via repression of *ICR1*.

The net effect of *FLO11*'s regulatory circuitry is the variegated transcription of its gene product in clonal wild-type (WT) cell populations: *FLO11* is expressed ("on") in some cells and is silenced ("off") in others (Halme et al., 2004; Bumgarner et al., 2009; Octavio et al., 2009). Expression of Flo11 protein on the yeast cell surface is required for haploid invasion and diploid filamentous growth, which have been understood as foraging responses that occur in nutrient-poor conditions (Roberts and Fink, 1994). Variegated *FLO11* expression results in phenotypic heterogeneity within clones because some genetically identical cells differentiate to form filaments that grow away from the founding colony, while others adhere to or invade local surfaces, and still others may wash away to more distant environments (Kaern et al., 2005).

Our previous study of the ncRNA toggle at *FLO11* relied on experimental techniques limited in their capacity to capture heterogeneity existing among individual cells in clonal populations. To obtain a more complete view of the roles of *ICR1* and *PWR1* in regulating *FLO11*, particularly in view of its variegated expression, we here use fluorescence in situ hybridization (FISH) and fluorescence microscopy to visualize simultaneously coding and noncoding RNA transcripts in fields of intact yeast

cells (Raj et al., 2006, 2008; Femino et al., 1998; Zenklusen et al., 2008; Raj and van Oudenaarden, 2008; Pena et al., 2009; Lu and Tsourkas, 2009). These single-cell studies have revealed insights about alternative expression states for *FLO11*. The data provide evidence at single-cell resolution that *ICR1* and *PWR1* contribute causally to *FLO11*'s variegated expression, exerting their effects by modulating the recruitment of key transcription factors (Liu et al., 1996; Pan and Heitman, 2002). Computational modeling combined with single-cell and bulk-cell experimental methods have revealed mechanistic aspects of the regulatory circuitry at *FLO11* and may prove useful for investigating roles of ncRNAs across eukaryotic organisms (Guttman et al., 2009; Huarte et al., 2010; Bertone et al., 2004; David et al., 2006; Davis and Ares, 2006; FANTOM Consortium, 2005; van Dijk et al., 2011).

RESULTS

Detection of *FLO11* Transcripts in Single Cells Reveals Alternative *FLO11* Expression States

RNA FISH experiments directly demonstrate that *FLO11* mRNA variegates in clonal populations of WT yeast (Figure 1B; see Figure S1 available online). Previous observations of *FLO11* variegation (Halme et al., 2004; Bumgarner et al., 2009; Octavio et al., 2009) relied upon indirect protein-based reporters. Here, we performed quantitative RNA FISH (Raj et al., 2008; Zenklusen et al., 2008) and fluorescence microscopy to detect *FLO11* mRNAs at single-cell resolution. Transcripts were imaged in situ in fields of clonal WT cells (Figure 1B). In z-dimensional image stacks, bound fluorescent probes appear as diffraction-limited dots within individual cells. Each dot, produced by collective binding of probes to target transcript, indicates a single RNA molecule (Femino et al., 1998, Raj et al., 2008). In analyses of >20,000 WT cells, *FLO11* dots were detected in 69% of cells (±1.6 standard error of the mean [SEM] calculated from four experiment replicates), while the remaining 31% (±1.4 SEM) of cells were devoid of *FLO11* dots (Figures 1D and 3D; Table 1).

The FISH microscopy images provide quantitative information about alternative *FLO11* expression states. We observe subpopulations of WT cells that exhibit no *FLO11* transcripts (0 dots), low-copy basal-level transcription (1–5 dots), or high-copy active transcription (>5 dots per cell; Figures 1D and 3D). Of cells in which *FLO11* transcripts are detected, 30% (±0.7 SEM) exhibit basal-level transcription and 39% (±0.8 SEM) are active for *FLO11* transcription, reproducibly containing ~30 mean transcripts per cell (Table 1).

Alternative *FLO11* expression states are also present in null mutants for *flo8*, Rpd3L$^-$ (i.e., *cti6*), and *sfl1*. Most *flo8* and *cti6* cells either contain no *FLO11* transcripts or exhibit basal-level transcription independent of these *trans*-activators (Figure 1D). Basal transcription is insufficient to support Flo11-dependent colony morphology (Figures 3C and 4D), adhesion, or filamentation (Bumgarner et al., 2009). In *sfl1*, 98% of cells are active for *FLO11* transcription (Figure 1D), containing on average 36 transcripts (±0.2 SEM) per cell (Table 1). The active cells in WT and *sfl1* populations contain similar numbers of *FLO11* transcripts (Table 1), suggesting that the overexpression of *FLO11* noted in population-based studies of *sfl1* (Pan and Heitman, 2002; Halme et al., 2004) is mainly due to an increase in the number of active *sfl1* cells rather than an increase in the number of transcripts per cell.

ncRNAs *PWR1* and *ICR1* Can Be Imaged In Situ in Single Cells

PWR1 and *ICR1* were also imaged in WT, *flo8*, *cti6*, and *sfl1* cells (Figures 1C and 1D and Figure S1). The ncRNAs are observed within nuclei and in cytoplasm (Figure 1C and Figure S1). They are detected in some cells within each clonal population but are completely absent in others, revealing variegation of *PWR1* and *ICR1* (Figure 1D). When either *PWR1* or *ICR1* is observed, we detect on average fewer than two transcripts per cell (Table 1), which may indicate intermittent transcription, low transcription rates, short half-lives, and/or technical limitations in our method of detection. Data collected from FISH experiments are largely consistent with previous observations from northern blots (Bumgarner et al., 2009). *PWR1* is detected more frequently in *sfl1* cells than in WT (Figure 1D), whereas *ICR1* is detected less often in *sfl1* cells than in WT (Figure 1D). In *cti6* and *flo8*, the percentage of cells containing *PWR1* is lower relative to both WT and *sfl1* (Figure 1D). *ICR1* is detected more often in *cti6* and *flo8* cells than in *sfl1*, but only the *cti6* mutant shows an increase in the percentage of cells in which *ICR1* is detected relative to WT (Figure 1D).

Simultaneous Imaging of *FLO11* and ncRNAs Supports Regulation of *FLO11* by *PWR1* and *ICR1*

FLO11 and ncRNAs were imaged simultaneously using spectrally distinct fluorophores. The coincidence of *FLO11* and *PWR1* transcripts in individual cells supports *PWR1*'s role in promoting *FLO11* expression (Figure 1C and Figure S1A). In active WT cells (i.e., cells containing >5 *FLO11* dots), there is a strong positive correlation between *PWR1* and *FLO11*. As *PWR1* count increases, the mean and median *FLO11* count also increases (Figure 2A). This observation deviates significantly from results expected under a null hypothesis in which *PWR1* and *FLO11* counts are independent (i.e., where *PWR1* count predicts no change in *FLO11* count, $\beta = 0$). Instead, using a linear regression model, the results are consistent with each *PWR1* dot predicting eight additional *FLO11* transcripts in a given cell (β = +8.2 *FLO11* per *PWR1*, 95% confidence interval [CI] = +6.9 to +9.5, p value = 1.99E-34).

Conditional on detection of *PWR1* in a given cell, the probability that the cell is also active for *FLO11* transcription is significantly higher than predicted under the null hypothesis (Table 2). To underscore this relationship, since ~40% of WT cells are active for *FLO11* transcription (Figures 1D and 3D), we would expect under the null hypothesis to find that ~40% of *PWR1*-positive cells are also active for *FLO11*. Instead, ~90% of *PWR1*-positive cells detected are also active for *FLO11* transcription, supporting a positive correlation (p value = 8.71E-65) between *PWR1* transcription and *FLO11* transcription (Table 2).

Simultaneous imaging of *FLO11* and *ICR1* in single cells supports *ICR1*'s role in repressing *FLO11* expression (Figure 1C and Figure S1B). Mean and median *FLO11* dot counts decrease

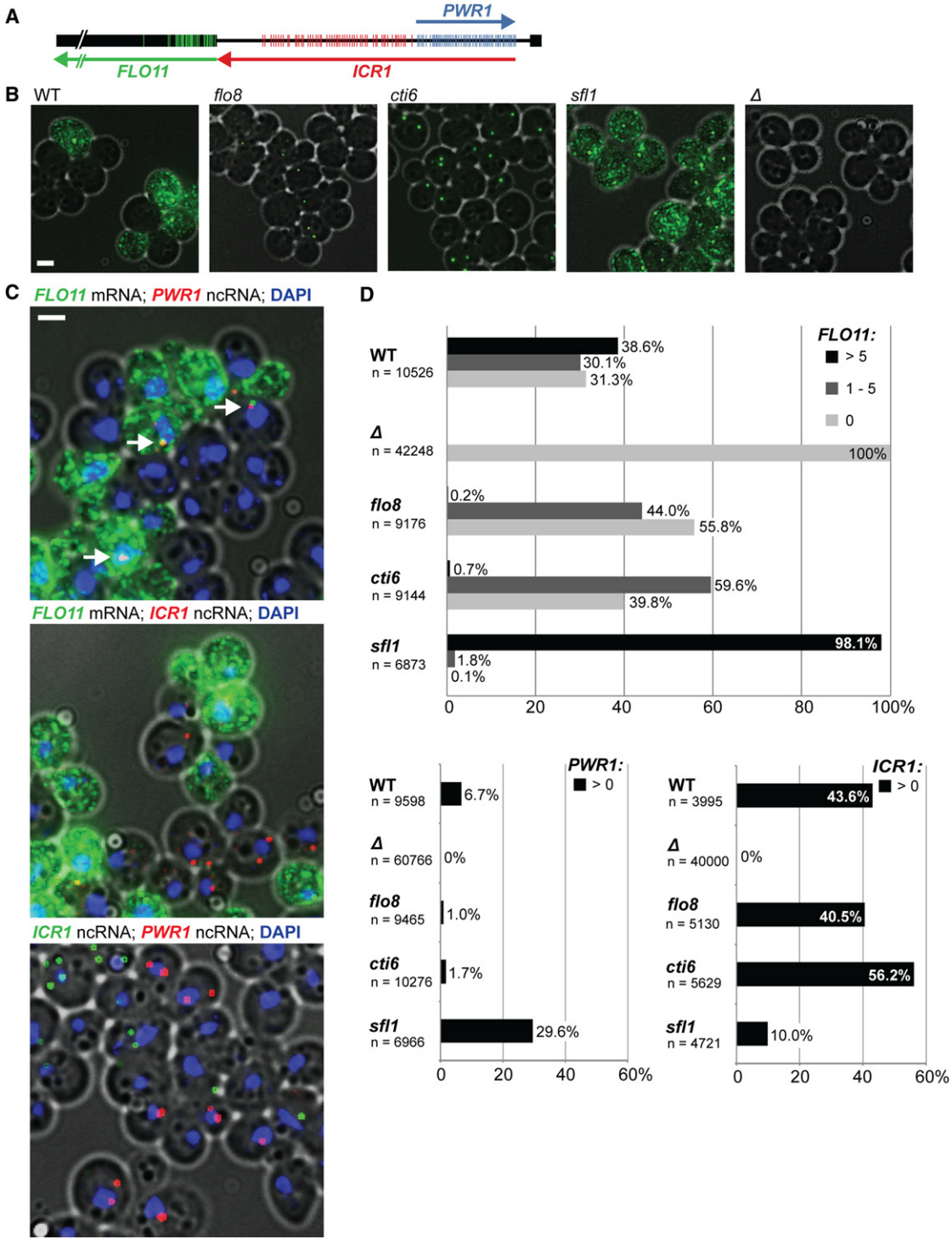

Figure 1. *FLO11*, *PWR1*, and *ICR1* Transcripts Detected using RNA FISH

(A) Vertical marks indicate genomic sequences of 20 nucleotide DNA probes used in RNA FISH experiments. See also the Supplemental Experimental Procedures.

(B) Probes coupled to tetramethylrhodamine (TMR) detect *FLO11* in WT (10560-6B), *flo8* (SBY1160), *cti6* (SBY591), and *sfl1* (SBY170) cells. In strain Δ (yCW91), the *FLO11* ORF and its entire promoter, including *PWR1* and *ICR1*, are deleted to control for probe specificity (scale bar, 2 μm).

(C) Merged fluorescence microscopy from FISH to detect two distinct transcript types simultaneously in WT cells. Images were selected from larger microscopy fields. Full image fields are shown in Figure S1. (Top) TMR-coupled probes detect *FLO11* (green dots), and Cy5-coupled probes detect *PWR1* (red dots). White arrows indicate colocalized high-intensity *FLO11* and *PWR1* dots, perhaps active transcription sites within DAPI-stained nuclei (scale bar, 2 μm). (Middle)

Table 1. The Mean Number, with Standard Error of the Mean and Standard Deviation, of Transcripts Detected per Cell in WT and Mutant Strains in Two Experiments, Each Twice Replicated

		FLO11 (>5)			*PWR1* (>0)			*ICR1* (>0)		
Genotype	Experiment	Mean ±SEM	SD	*f*	Mean ±SEM	SD	*f*	Mean ±SEM	SD	*f*
WT	1	28.6 ± 0.3	16.3	4,062/10,526	1.2 ± 0.1	0.4	644/9598	1.5 ± 0.1	1.6	1,741/3,995
Δ	1	0	-	2/42248	0	-	1/60,766	0	-	0/40,000
flo8	1	14.7 ± 2.4	10.9	20/9176	1.8 ± 0.2	1.8	99/9,465	1.5 ± 0.1	1.8	2,079/5,130
cti6	1	24.8 ± 3.9	29.8	60/9144	2.0 ± 0.2	3.1	178/10,276	1.7 ± 0.1	2.0	3,161/5,629
sfl1	1	36.2 ± 0.2	15.7	6,739/6,873	1.2 ± 0.1	0.5	2,059/6,966	1.9 ± 0.2	4.2	474/4,721
WT	2	26.5 ± 0.3	16.3	4,212/10,730						
cti6	2	10.3 ± 0.7	15.1	473/13,273						
cti6 pMET-ICR1	2	32.1 ± 0.5	21.9	1,996/15,751						
cti6 ΔpICR1	2	34.7 ± 0.6	22.2	1,609/11,187						
cti6 icr1::Term	2	37.0 ± 0.8	24.7	1,016/14,407						

Results for *FLO11* (>5 dots), *PWR1* (>0 dots), and *ICR1* (>0 dots) transcripts are given for experiment 1. Only *FLO11* was assayed in experiment 2. In strain Δ, the *FLO11* ORF and its ~3.6 kb promoter are deleted. For each experiment, the frequency of cells containing the indicated transcript is given by *f*. SD, standard deviation.

as *ICR1* dot count increases (Figure 2B). Linear regression analysis of the full data set (Figure 2B) yields a model in which each *ICR1* dot predicts two fewer *FLO11* dots in a cell (β = −2.1 *FLO11* per *ICR1*, 95% CI = −1.0 to −3.1, p value = 1.54E-04). The presence of two or more *ICR1* dots is coincident with marked reduction in *FLO11* (Figure 2B). Linear regression analysis of the subset of cells in which two or more *ICR1* dots are detected (Figure 2B) predicts four fewer *FLO11* dots per *ICR1* (β = −4.1 *FLO11* per *ICR1*, 95% CI = −1.3 to −6.9, p value = 0.0049). *FLO11* and *ICR1* dots are coincident in some cells (Figure 1C and Figure S1B), but it is not possible to discern from our data whether these cells were actively transcribing both transcripts or had undergone a recent switching event.

Simultaneous imaging of *PWR1* and *ICR1* ncRNAs in individual cells supports the existence of a ncRNA toggle (Bumgarner et al., 2009; Figures 1C and 2C and Figure S1C). Under a null hypothesis in which these ncRNAs are independent, the number of *PWR1* dots is not expected to correlate with the number of *ICR1* dots. Instead, we observe a significant decrease in the mean number of *ICR1* dots detected as the number of *PWR1* dots increases in WT and *sfl1* cells (Figure 2C). This effect is observed when cells are binned according to *PWR1* count and then mean and 95% CI are determined for each binned population's *ICR1* counts (Figure 2C). Linear regression performed on the full set of WT cells (Figure 2C) shows that each *PWR1* dot predicts one fewer *ICR1* transcript within a given cell (β = −0.9 *ICR1* per *PWR1*, 95% CI = −0.7 to −1.1, p value = 5.86E-22). Analysis of the subset of WT cells that contain either zero or one *PWR1* dot (i.e., comparing the bins between which the greatest change in *ICR1* is observed [Figure 2C]) reveals a marked reduction in *ICR1* count predicted by the presence of *PWR1* (β = −1.2 *ICR1* per *PWR1*, 95% CI = −1.0 to −1.5, p-value = 1.84E-21). Linear regression performed on the full *sfl1* population summarized in Figure 2C shows that each *PWR1* dot predicts one fewer *ICR1* transcript within a cell (β = −0.8 *ICR1* per *PWR1*, 95% CI = −0.7 to −1.0, p value = 1.30E-25). When only the subset of *sfl1* cells that contain either zero or one *PWR1* dot are analyzed, an even greater reduction in *ICR1* is predicted by the presence of *PWR1* (β = −1.9 *ICR1* per *PWR1*, 95% CI = −1.6 to −2.2, p value = 1.09E-39). *ICR1* and *PWR1* are sometimes observed together in cells (Figure 2C and Figure S1C), which may be indicative of recent switches of the toggle (i.e., where one ncRNA is being newly synthesized while the other persists because it has not yet been degraded).

Reduction of *ICR1* Recovers Cells Active for *FLO11* Transcription

Transcription of *ICR1* was reduced via three distinct methods in the *cti6* mutant. One method uses a transcriptional terminator to disrupt *ICR1* (*icr1::Term*, T3 in Bumgarner et al., 2009). Another (*cti6 ΔpICR1*) reduces *ICR1* transcription by removing the ncRNA's upstream regulatory sequences (Figure S2). The third (*cti6 pMET-ICR1*) controls *ICR1* under the *MET25* promoter (Figures 3 and 4), which is repressed in rich media and induced in media lacking methionine.

Decreasing *ICR1* transcription by any of these approaches increases *FLO11* expression in bulk-cell assays (Figure 3A) and restores Flo11-dependent colony morphology (Figure 3C). In all three cases, FISH experiments show that reduction of *ICR1* recovers cells active for *FLO11* transcription (Figures 3C and

TMR-coupled probes detect *FLO11* (green dots), and Cy5-coupled probes detect *ICR1* (red dots). (Bottom) TMR-coupled probes detect *ICR1* (green dots), and Cy5-coupled probes detect *PWR1* (red dots).

(D) (Top) FISH reveals different *FLO11* expression states. Histogram shows the percentage of cells from each clonal population that contains (i) >5 *FLO11* dots (active), (ii) 1–5 dots (basal), and (iii) 0 dots (inactive or silenced). Total number of cells assayed is given by n for each genotype. (Bottom left) The percentage of cells in which *PWR1* (>0 dots) is detected. (Bottom right) The percentage of cells in which *ICR1* (>0 dots) is detected.

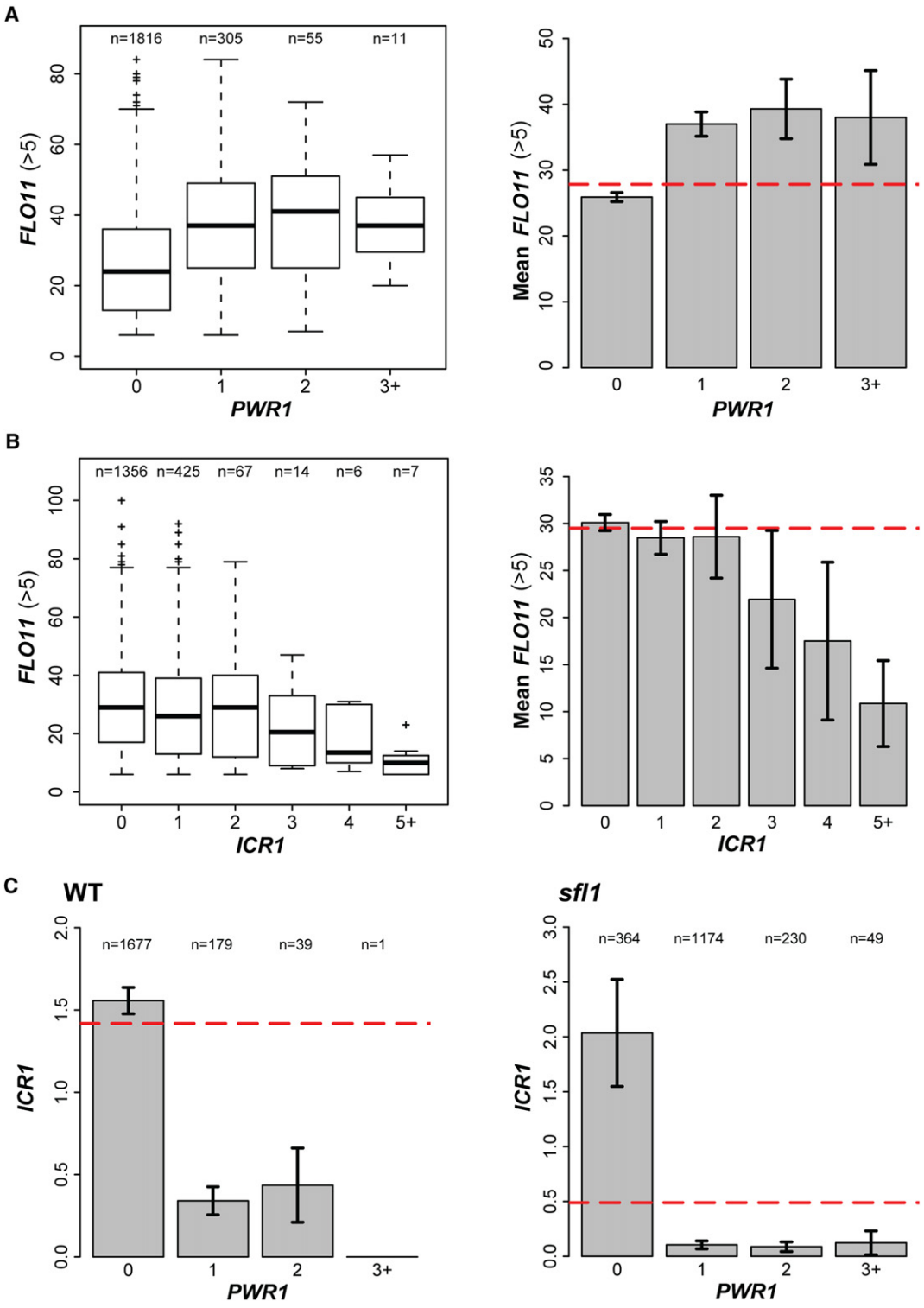

Figure 2. Single-Cell Assays Reveal Correlations among *FLO11*, *PWR1*, and *ICR1* Transcripts that Support a ncRNA Toggle Involved in *FLO11* Regulation

(A) The box-and-whisker plot (left) summarizes the distribution of *PWR1* in WT cells that are active (i.e., contain >5 *FLO11* dots) for *FLO11* transcription. Median *FLO11* count is indicated by the thick horizontal bar for each *PWR1* bin. Boxes give counts for upper and lower population quartiles. Whiskers show maximum and minimum transcript counts. Crosses represent outliers (i.e., >1.5× upper quartile or <1.5× lower quartile). The cell count in each *PWR1* bin is given by n. The histogram (right) gives mean *FLO11* count versus *PWR1* count in individual WT cells that are active for *FLO11* transcription. Error bars provide 95% confidence

Table 2. When *PWR1* Is Also Detected, High-Copy *FLO11* Transcripts Are Present in Cells More Often Than Predicted by Chance

		Percentage of Cells in Population with		If *PWR1* > 0, then Also *FLO11* > 5?			
Genotype	n	*FLO11* > 5	*PWR1* > 0	Under Null, Expected	Observed	Fold Increase	P Value
WT	10,730	39.25%	2.68%	39.25%	87.50% (252/288)	2.23×	8.71E-65
cti6	13,273	3.56%	0.69%	3.65%	13.04% (12/92)	3.57×	8.57E-07
cti6 pMET-ICR1	15,751	12.67%	0.89%	12.67%	60.71% (85/140)	4.79×	4.93E-66
cti6 ΔpICR1	11,187	14.38%	1.68%	14.38%	67.55% (127/188)	4.70×	1.80E-97
cti6 icr1::Term	14,407	7.05%	1.58%	7.05%	67.40% (153/227)	9.56×	1.22E-280

Pearson's chi-square analyses to generate p values were conducted under the null hypothesis that *PWR1* and *FLO11* transcription are independent. Total number of imaged cells is given by n.

3D). The number of *FLO11* transcripts detected in rescued active cells (~30 dots per cell) is similar to the number observed in active WT and *sfl1* cells (Table 1). Thus, reduction of *ICR1* transcription in the *cti6* mutant restores a subpopulation of active cells that is indistinguishable in quality, although different in population frequency, compared to active cells observed in WT.

Bulk-cell assays reveal that average *FLO11* levels are elevated but not fully returned to WT when *ICR1* transcription is reduced in the *cti6* background (Figure 3A). Several models could explain this observation (Figure 3B). In model 1, the same percentage of cells is "on" in WT and the rescued strain, but WT cells express *FLO11* more highly. In model 2, a smaller percentage of cells turns "on" in the rescued population, but each rescued cell expresses *FLO11* at a level similar to WT active cells. In model 3, reduction of *ICR1* enables all cells in the rescued population to express *FLO11*, but each at a very low level. Single-cell imaging enabled distinction among these models, showing that model 2 is most appropriate to explain the observed phenomena. These results suggest that an additional *ICR1*-independent repressor is also dysregulated in the *cti6* mutant. The additional repressor may be Sfl1, which shows enriched recruitment to the *FLO11* promoter in the *cti6* mutant compared to WT (Figure 5D).

When *ICR1* transcription is reduced in *cti6*, *PWR1* is detected in a higher percentage of cells compared to the unmodified *cti6* cell background (Table 2). Conditional on detection of *PWR1* in a given cell, the probability of high-copy *FLO11* transcripts being detected in that same cell is significantly higher than expected if *PWR1* and *FLO11* transcription were independent events (Table 2). For example, 14% of *cti6 ΔpICR1* cells are active for *FLO11* transcription (Table 2). Thus under the null hypothesis, 14% of *PWR1*-positive cells would be expected to be active for *FLO11* transcription. Instead, we see that 68% of *PWR1*-positive cells are active for *FLO11* transcription (mean dot count, 35 ± 0.6 SEM; Table 1), a significant 4.7-fold increase over the expectation under the null (p value = 1.80E-97) (Table 2).

An examination of the shifting distributions of alternative *FLO11* expression states (Figure 3D) suggests that, when *ICR1* transcription is reduced in *cti6*, the rescued subpopulation of active cells may be derived mainly from the subpopulation of basal cells. This observation raises the possibility that, rather than playing a direct role in modulating silencing of *FLO11* transcription, the ncRNA toggle plays a role in the switch from basal to active state. This idea is further supported by northern analysis that shows that the Hda1 HDAC does not affect *ICR1* transcription (Figure S4F), suggesting that Hda1-mediated silencing (Halme et al., 2004; Octavio et al., 2009) occurs downstream or independently of *ICR1*-mediated *FLO11* repression.

Induction of *ICR1* Transcription Decreases *FLO11* Transcription

To investigate further the effect of *ICR1* on *FLO11* expression, heterologous promoters (Janke et al., 2004) were inserted to control *ICR1* transcription. Increased *ICR1* transcription under *TEF* (*pTEF*) or *GPD1* (*pGPD*) promoters results in decreased *FLO11* in WT and *sfl1* (Figures 4A–4C) and loss of Flo11-dependent colony morphologies—a particularly striking result for the *sfl1* mutant which normally produces very crinkly colonies (Figure 4D). Conversely, reduction of *ICR1* under the *MET25* promoter (*pMET*), which is repressed in YPD, results in elevated *FLO11* transcript levels and restores crinkled colony morphology to the *cti6* mutant (Figure 4). In contrast, when *pMET-ICR1* strains are grown in synthetic media that lacks methionine (i.e., when the *pMET* promoter is induced), we observe the inverse effect: a reduction of *FLO11* transcript levels (Figure 4C).

intervals (CIs) on estimated mean *FLO11* counts. The red dashed line indicates the expected distribution of *FLO11* under a null hypothesis in which *PWR1* and *FLO11* counts are independent (i.e., where β, the effect or degree to which *PWR1* count predicts *FLO11* count in a given cell, equals zero).

(B) The box-and-whisker plot (left) summarizes the distribution of *ICR1* in WT cells that are active for *FLO11* transcription. The histogram (right) gives mean *FLO11* count versus *ICR1* count in WT cells that are active for *FLO11* transcription. Error bars show 95% CIs on estimated mean *FLO11* counts. The red dashed line indicates the expected distribution of *FLO11* under a null hypothesis in which *ICR1* and *FLO11* counts are independent (β = 0).

(C) Histograms show mean *ICR1* count versus *PWR1* count in WT (left) and *sfl1* (right) cells. Error bars provide 95% CIs on estimated mean *ICR1* counts. The red dashed lines indicate the expected distributions of *ICR1* under a null hypothesis in which *PWR1* and *ICR1* are independent (β = 0). These analyses utilized cells containing at least one *PWR1* or *ICR1* dot, since cells devoid of both ncRNAs are not informative to assess the toggle (Bumgarner et al., 2009). Cells that contained no *PWR1* dots but at least one *ICR1* dot were binned, and then mean and 95% CI were determined for *ICR1* in that population. Then cells containing one *PWR1* transcript were binned and the mean and 95% CI were determined for *ICR1* in that population of cells, etc. Cell count in each bin is given by n.

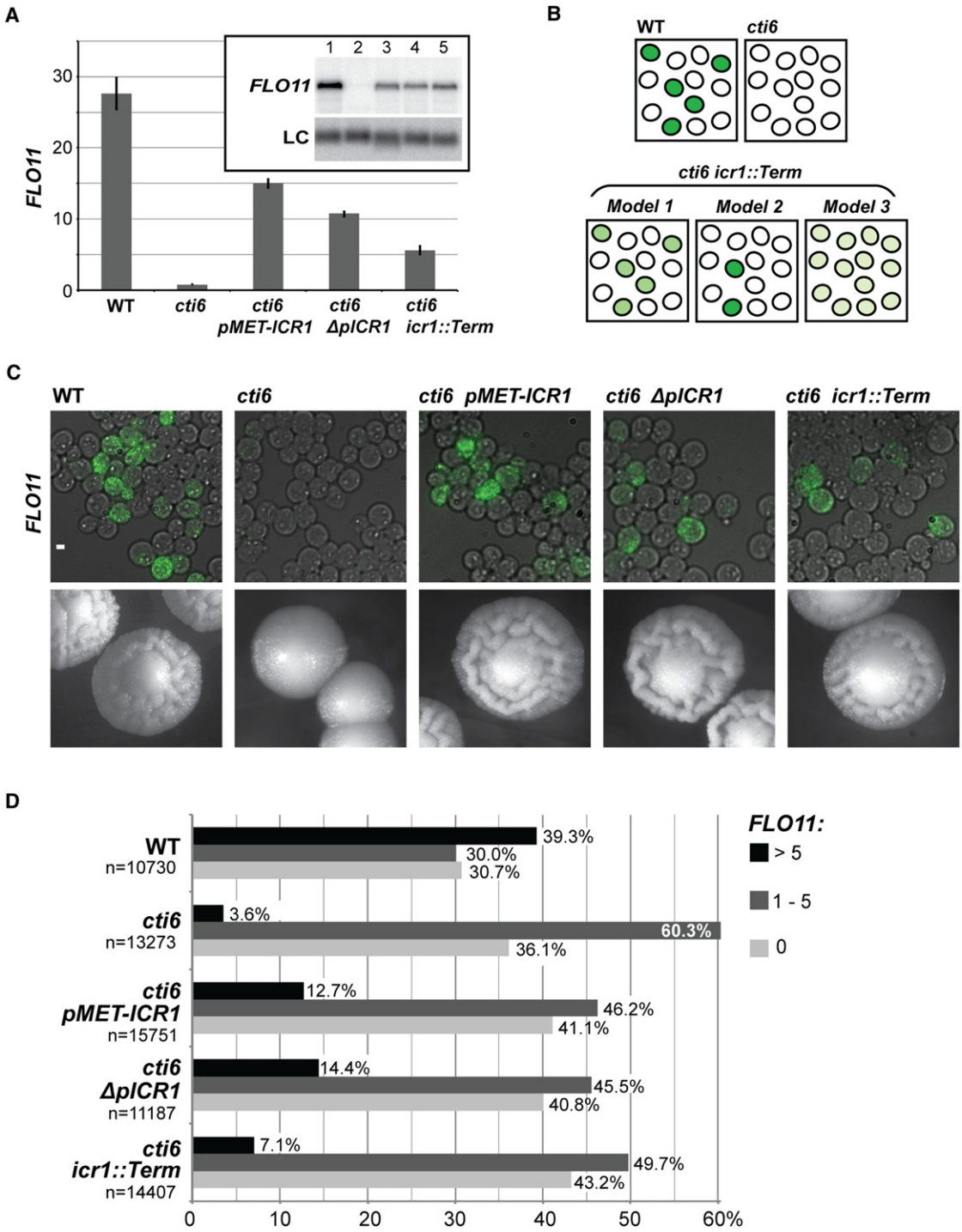

Figure 3. Reducing *ICR1* Transcription in the Rpd3L⁻ (*cti6*) Mutant Recovers Cells with Active *FLO11* Transcription

ICR1 transcription was reduced by three methods: (1) insertion of the *MET25* promoter, repressed in rich media, to control transcription of *ICR1* (*pMET-ICR1*) from its endogenous site, (2) deletion of 100 bp of DNA sequence located immediately upstream of the mapped *ICR1* start site (*ΔpICR1*; Bumgarner et al., 2009) and required for *ICR1*'s repression of *FLO11* (see Figure S2), and (3) insertion of a transcriptional terminator (*icr1::Term*; T3 in Bumgarner et al., 2009).

(A) Quantitative PCR (qPCR) assay of *FLO11* mRNA in haploids, normalized to *ACT1* and presented ±SD. (Inset) *FLO11* mRNA assayed by northern blot. Lane 1, WT; lane 2, *cti6*; lane 3, *cti6 pMET-ICR1*; lane 4, *cti6 ΔpICR1*; lane 5, *cti6 icr1::Term*.

(B) Alternative models to explain the observation that *FLO11* is not returned to mean WT levels when *ICR1* is disrupted in the *cti6* background. (Model 1) The percentage of "on" cells is the same in WT and rescued population, but *FLO11* is expressed at a lower level in rescued cells. (Model 2) The percentage of "on" cells is higher in WT than in the rescued population, but every "on" cell expresses *FLO11* at a similar level. (Model 3) All cells in the rescued population express *FLO11* at a low level.

ICR1 Transcription Controls Recruitment of Key Transcription Factors to the *FLO11* Promoter

The distribution of *FLO11* counts detected in the WT population can be reconstituted by combining the distributions observed in *flo8* and *sfl1* mutants (Figure 5A). Furthermore, recruitment of Flo8 to the *FLO11* promoter is reduced in the *cti6* mutant and increased in the *sfl1* mutant (Bumgarner et al., 2009). These results provoked further examination of the relationship between *ICR1* transcription and the recruitment of key *trans*-acting factors to the *FLO11* promoter.

ICR1 transcription inhibits recruitment of Flo8 and Sfl1 to the *FLO11* promoter. When *ICR1* transcription is reduced in the *cti6* mutant (Figure 3), there is a marked increase in the recruitment of Flo8 (Figure 5B) to its binding region (Pan and Heitman, 2002). ChIP performed on strains in which heterologous promoters increase *ICR1* transcription reveal reduced recruitment of myc-tagged Flo8 and Sfl1 to the *FLO11* promoter (Figures 5C and 5D). Repression of *ICR1* transcription under *pMET* when WT and mutant strains are grown in rich media results in the enrichment of myc-tagged Flo8 and Sfl1 to the *FLO11* promoter (Figures 5B–5D). These data demonstrate that *ICR1* transcription interferes with recruitment, occluding (Martens et al., 2004) or ejecting these *trans*-acting factors from the *FLO11* promoter.

We developed a computational framework that captures the changes in measured *FLO11* transcript distributions observed across genotypes as a function of recruited Flo8 transcription factor. A mixture model (McLachlan and Peel, 2000) assumes two populations of cells, one with no Flo8 recruitment that exhibits basal/low *FLO11* expression and another with maximum Flo8 recruitment that exhibits high-copy active *FLO11* expression. The parameters for the population of cells with no Flo8 recruitment were determined empirically using the *flo8* deletion strain. The *FLO11* transcript distribution in *flo8* is best fit with a Poisson distribution using maximum likelihood optimization (Figure 5E). The parameters for the population of cells with maximum Flo8 recruitment were determined using the *sfl1* deletion strain. In *sfl1*, a gamma distribution is the best fit for the measured *FLO11* transcript distribution (Figure 5E). Once parameters were determined from these fits, the mixture model was constrained to one free parameter, namely the fraction of cells exhibiting high-copy *FLO11* transcript expression. We fit the mixture model to *FLO11* transcript distributions observed in WT, *cti6*, *cti6 ΔpICR1*, and *cti6 pMET-ICR1* strains (Figure 5E and Figure S3). A strong positive correlation (Figure 5F) is observed between the amount of Flo8 recruitment measured by ChIP and the fraction of cells exhibiting high-copy *FLO11* transcripts within a given population. This combination of experimental and computational approaches supports the hypothesis that the ncRNA *ICR1* modulates alternative *FLO11* expression states by controlling Flo8 recruitment to the *FLO11* promoter (Figure 5G).

DISCUSSION

Single-cell resolution FISH imaging has revealed alternative *FLO11* expression states that were not detectable by other methods (Halme et al., 2004; Bumgarner et al., 2009; Octavio et al., 2009) and directly demonstrate that *FLO11* mRNA *itself* variegates in clonal populations (Figures 2 and 3 and Figure S1). In WT, one class of cells is devoid of *FLO11* transcripts, suggesting transcriptional inactivity or silencing at *FLO11*. A second class contains one to five transcripts per cell, exhibiting low-level basal *FLO11* transcription. The third class is active for *FLO11* transcription, with a mean count of ~30 *FLO11* transcripts per cell (Table 1). Thus, Flo11-dependent phenotypic heterogeneity observed in WT clones results from substantial cell-to-cell differences in *FLO11* expression rather than noisy low-level expression across the population.

The three classes of cells may represent alternative promoter states predicted computationally to exist at *FLO11* (Octavio et al., 2009) and demonstrated experimentally at other loci (Vermaak et al., 2003; Li et al., 2007): a silent promoter state mediated by local chromatin structure, a competent but inactive or basal promoter state resulting from absence of required *trans*-activators or presence of *trans*-acting repressors, and an active promoter state. The importance of such alternative states in cellular differentiation is clear for multicellular organisms, composed of genetically homogeneous cells that are structurally and functionally heterogeneous due to differential gene expression. These alternative expression states also have biological significance for clones of unicellular yeast. They explain the phenomenon of Flo11-dependent phenotypic variegation (Halme et al., 2004) that may provide a survival advantage, not to individual cells per se, but to the clone's genetic identity by promoting survival in fluctuating environmental conditions (Büttner et al., 2006; Batada and Hurst, 2007; Acar et al., 2008; Lehner, 2008).

The distinction discerned between the basal (1–5 dots) and active (>5 dots) expression states of *FLO11* is biologically meaningful. Flo8 is recognized as the key activator for *FLO11*, and null alleles of *flo8* or *cti6* exhibit loss of Flo11-dependent phenotypes such as haploid adhesion, crinkly colony morphology, and diploid filamentation (Figures 3 and 4; Liu et al., 1996; Guo et al., 2000; Bumgarner et al., 2009). Yet *flo8* and *cti6* mutant populations contain many cells that exhibit basal-level expression (Figure 1D), demonstrating that ≤5 copies of *FLO11* per cell is insufficient to support Flo11-dependent phenotypes.

Single-cell resolution has revealed mechanistic aspects of the regulatory circuitry at *FLO11* that would not have been discernable using population-wide measurements. Reduction of *ICR1* transcription in the *cti6* mutant causes a subset of cells to recover active transcription (Figures 4C and 4D), pointing to a causal role for *ICR1* in repressing active *FLO11* expression in individual cells. Together, empirical results and computational

(C) (Top row) *FLO11* detected with TMR-coupled probes in WT (10560-6B), *cti6* (SBY591), *cti6 pMET-ICR1* (SBY1636), *cti6 ΔpICR1* (SBY1523), and *cti6 icr1::Term* (SBY1182) cells (scale bar, 2 μm). (Bottom row) Reduction of *ICR1* transcription restores WT crinkly colony morphology to haploid *cti6* mutants (4 days on YPD-agar at 30°C).

(D) The histogram shows the percentage of cells that contain *(i)* >5 *FLO11* dots (active), *(ii)* 1–5 dots (basal), and *(iii)* 0 dots (inactive or silenced). Total number of imaged cells is given by n.

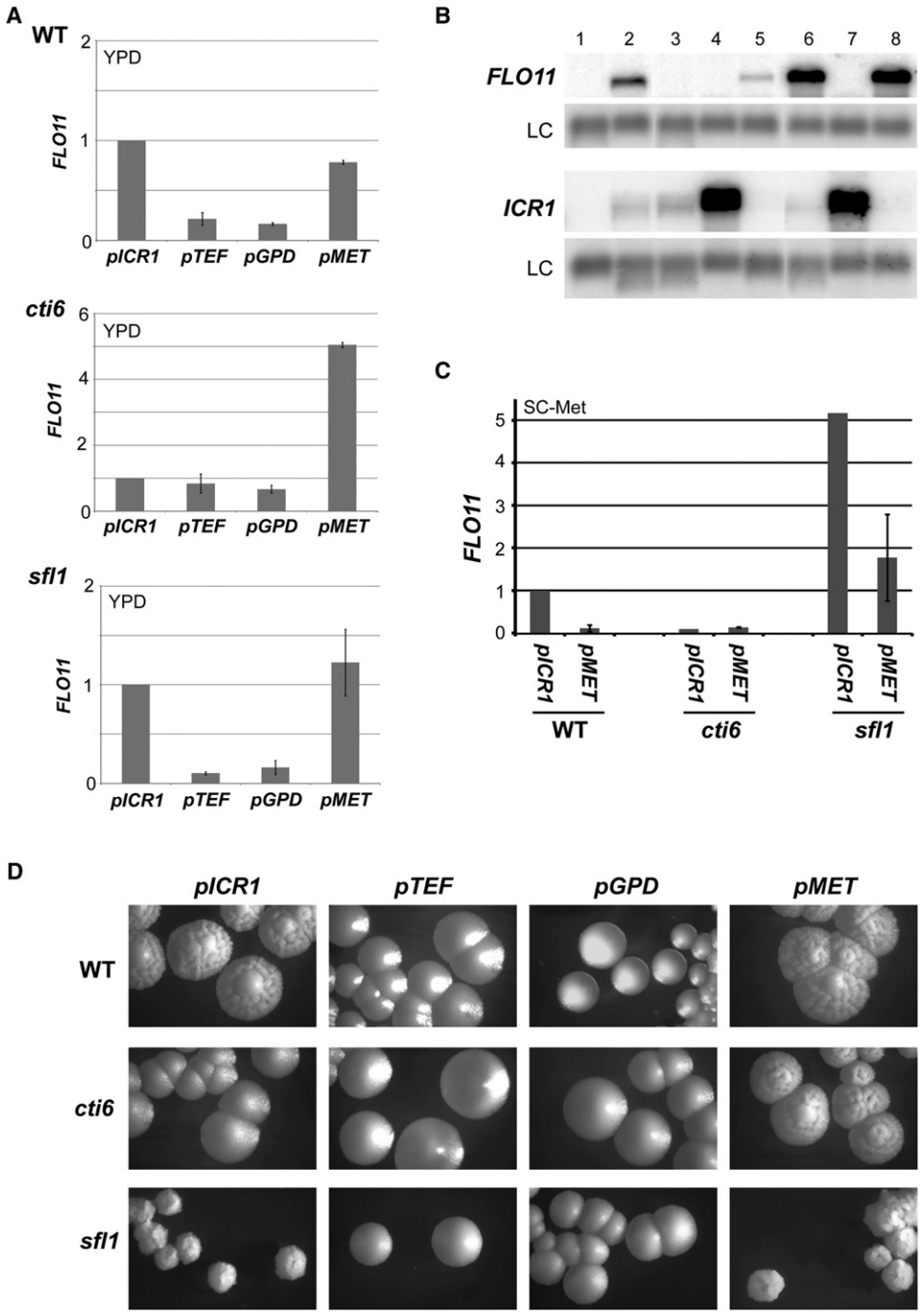

Figure 4. Modulating *ICR1* Transcription with Heterologous Promoters Alters *FLO11* Expression and Flo11-Dependent Phenotypes

Haploid strains in which upstream sequences that control *ICR1* transcription have been replaced with one of three different heterologous promoters: *pTEF* (*TEF* promoter; pYM-N19), *pGPD* (*GPD1* promoter; pYM-N15), or *pMET* (*MET25* promoter; pYM-N35) (Janke et al., 2004). *pICR1* indicates the unmodified endogenous WT DNA sequences upstream of *ICR1*.

(A) qPCR assays of *FLO11* mRNA, normalized to *ACT1* and presented as fold-change relative to genotype-matched strain carrying unmodified *pICR1* ±SD (WT strains: 10560-6B, SBY1642, SBY1639, SBY1648; *cti6* strains, SBY591, SBY1630, SBY1627, SBY1636; *sfl1* strains: SBY170, SBY1618, SBY1615, SBY1624).

(B) *FLO11* and *ICR1* assayed by northern blot with strand-specific RNA probes. Lane 1, *Δ*; lane 2, WT; lane 3, *cti6*; lane 4, *cti6 pGPD-ICR1*; lane 5, *cti6 pMET-ICR1*; lane 6, *sfl1* ; lane 7, *sfl1 pGPD-ICR1*; lane 8, *sfl1 pMET-ICR1*.

(C) qPCR assays of *FLO11* mRNA in haploid strains grown in liquid synthetic media lacking methionine (SC-Met), a condition that induces *pMET*. Results normalized to *ACT1* and presented as fold-change of WT level ±SD.

(D) Colony morphologies of strains carrying unmodified *pICR1* or indicated heterologous promoter driving *ICR1* (4 days on YPD-agar at 30°C).

modeling suggest that *ICR1*'s repressive effect is due to occlusion or ejection of key *trans*-acting factors Flo8 and Sfl1 (Figure 5; Martens et al., 2004; Bumgarner et al., 2009) from their respective binding sites on the *FLO11* promoter (Pan and Heitman, 2002). Since *PWR1* is not detected in every cell that is active for *FLO11* transcription (Figure 2A) and *ICR1* is not detected in every cell that is "off" for *FLO11* (Figure 2B), these ncRNAs might not be required to maintain alternative *FLO11* transcription states but could instead help transition the locus between states.

Previous results (Bumgarner et al., 2009) show that *ICR1* and *PWR1* exert their effects on *FLO11* and on each other via a *cis*-acting process. Thus, the process of transcription, rather than the products of the transcriptional process, is mechanistically important for the toggle. Transcription of *ICR1* along the length of the *FLO11* promoter may serve to "reset" the promoter by transiently eliminating interactions between the DNA and *trans*-acting activators and repressors, such that Flo8 and Sfl1 compete anew for recruitment to the *FLO11* promoter (Figure 5G). *ICR1* transcription may thereby influence the likelihood of downstream events that lead to an active or inactive *FLO11* transcription state. The competitive binding of Sfl1 or Flo8 (Pan and Heitman, 2002) is also central to the toggle. Their recruitment is influenced by the activity of Rpd3L (Figure 5) and feeds back to determine which ncRNA transcript program is initiated. Sfl1 initiates a cascade of events that result in reversible transition to the silenced state (Halme et al., 2004), whereas Flo8 initiates events that transition the *FLO11* promoter from basal to active state. Our studies suggest that recruitment of Flo8 induces a pulse of *PWR1* transcription that promotes the *FLO11* active state by interfering in *cis* with *ICR1* transcription (Figure 5G).

Quantitative RNA FISH assays in single cells, genetic analysis, and computational modeling together have power to provide unanticipated insights into the *cis*-acting roles of ncRNAs. The integration of experimental techniques used in this study has enabled a quantitative understanding of the function of long ncRNAs in gene regulation in yeast and may prove to be a useful strategy for investigating these transcripts across organisms.

EXPERIMENTAL PROCEDURES

Strains, Media, Microbiological Techniques, and Growth Conditions

Yeast strains (see the table provided in the Supplemental Experimental Procedures) were derived from Σ1278b (Liu et al., 1996). Standard media were prepared and genetic manipulation techniques were carried out as described (Guthrie and Fink, 2002). Deletions of the endogenous *ICR1* promoter region were generated as described in Figure S2 (Güldener et al., 1996). NatR-marked promoters *pTEF* (pYM-N19), *pGPD1* (pYM-N15), and *pMET25* (pYM-N35) were integrated 3,446 bp upstream of the *FLO11* ATG, without loss of endogenous sequence, to control *ICR1* (Janke et al., 2004). For northern blot analysis, qPCR, and ChIP, cells were grown overnight at 30°C in YPD liquid, diluted to OD_{600}0.1, and all cultures grown to either OD_{600}0.8–1.2 or OD_{600}2.8–3.0.

RNA Fluorescence In Situ Hybridization

RNA FISH was performed as described (Raj et al., 2008), with the following modifications: yeast cultures were grown at 30°C in YPD liquid from starting concentration OD_{600}0.1 to final concentration OD_{600}2.8–3.0. Formaldehyde fixation was performed for 30 min at 22°C and continued overnight at 4°C, with gentle rocking throughout. Zymolyase digestions were performed at 30°C in TV 500 μl buffer B containing 8 μl zymolyase (2.5 mg/ml) for 1.25 hr while rotating tubes. Hybridizations with DNA probes (Figure 1A and the table provided in the Supplemental Experimental Procedures) were performed in 10% formamide hybridization buffer. *FLO11*-specific probes were coupled to TMR, *PWR1*-specific probes were coupled to Cy5, and *ICR1*-specific probes were coupled to either TMR or Cy5. To protect fluorophores from oxidation during imaging, cells were suspended in GLOX buffer as described (Raj et al., 2008) and imaged on standard glass microscope slides using coverslips sealed with silicon gaskets.

Fluorescence Microscopy Image Acquisition and Analysis

Images were collected using a Nikon TE2000 inverted fluorescence microscope with 100× oil-immersion objective, appropriate filters (TMR, Cy5, and DAPI), and a Princeton Instruments camera with MetaMorph software (Molecular Devices, Downington, PA). Custom filter sets were designed to distinguish TMR and Cy5 signal. Differential interference contrast (DIC), DAPI, TMR, and Cy5 images were collected with 0.2 micron z slices. DIC and DAPI images were used to identify individual cells. TMR and Cy5 image stacks were used to detect RNA transcripts. For image processing, a DIC image was chosen in which a clear cell boundary could be observed. This image was converted into a binary image using automated thresholding. The maximum projection of a DAPI image stack was generated and converted into a binary image using a fixed pixel intensity threshold. The binary DIC image was merged with the binary DAPI image. DAPI-stained nuclei were used in running a marker-controlled watershed algorithm over the merged DIC/DAPI image. Cell boundaries of individual cells were obtained using an edge-detection algorithm. Connected regions measuring larger than the expected range of sizes for an individual cell were rejected. The number of RNA transcripts in each cell was counted using a program that operates as follows: to enhance particulate signals, the program runs a median filter followed by a Laplacian filter on each optical slice. A threshold was then selected to detect individual dots in each plane. The particle count was robust over a range of selected thresholds. Images that demarcated cell boundaries were merged with each plane of TMR or Cy5 image stacks. This processing enabled the program to count the total number of isolated signals in three dimensions within each cell.

Northern Blot Analysis

Total RNA was isolated by standard acid phenol extraction and oligo(dT) selected (QIAGEN Oligotex mRNA Kit) to enrich for polyadenylated transcripts. RNAs were separated on formaldehyde-agarose denaturing gels and blotted as described (Sambrook et al., 1989). Hybond membranes (Amersham) were hybridized with strand-specific ^{32}P-labeled RNA probes generated using the Ambion T7 Maxiscript Kit. For load controls, a ^{32}P (exo-) Klenow-labeled DNA probe specific to transcript *SCR1* was used, with the exception of the blot in Figure S4F, in which a ^{32}P (exo-) Klenow-labeled DNA probe specific to transcript *TPI1* was used.

qPCR

Total RNA obtained by standard acid phenol extraction was reversed transcribed (QIAGEN QuantiTect Kit). cDNAs were analyzed with specific primers, SYBR Green reagents (Applied Biosystems), and the ABI 7500 qPCR system.

ChIP

Protocols have been described (Lee et al., 2006). Briefly, IPs were performed with Dynal Protein G magnetic beads preincubated with antibody against Myc-epitope (Covance 9E-11 MMS-164P). SYBR Green qPCR (Applied Biosystems) was performed on IP and WCE with specific primers.

Statistical Analyses

For regression analyses, where *FLO11* transcript count (the outcome variable) was regressed against *PWR1* or *ICR1* transcript number (the predictor variable), a log-additive model relating the predictor to the outcome was assumed. Linear regression was performed with the statistical software package R using the glm() function. For the other tests of independence between the transcripts, a standard Pearson's chi-square test was performed.

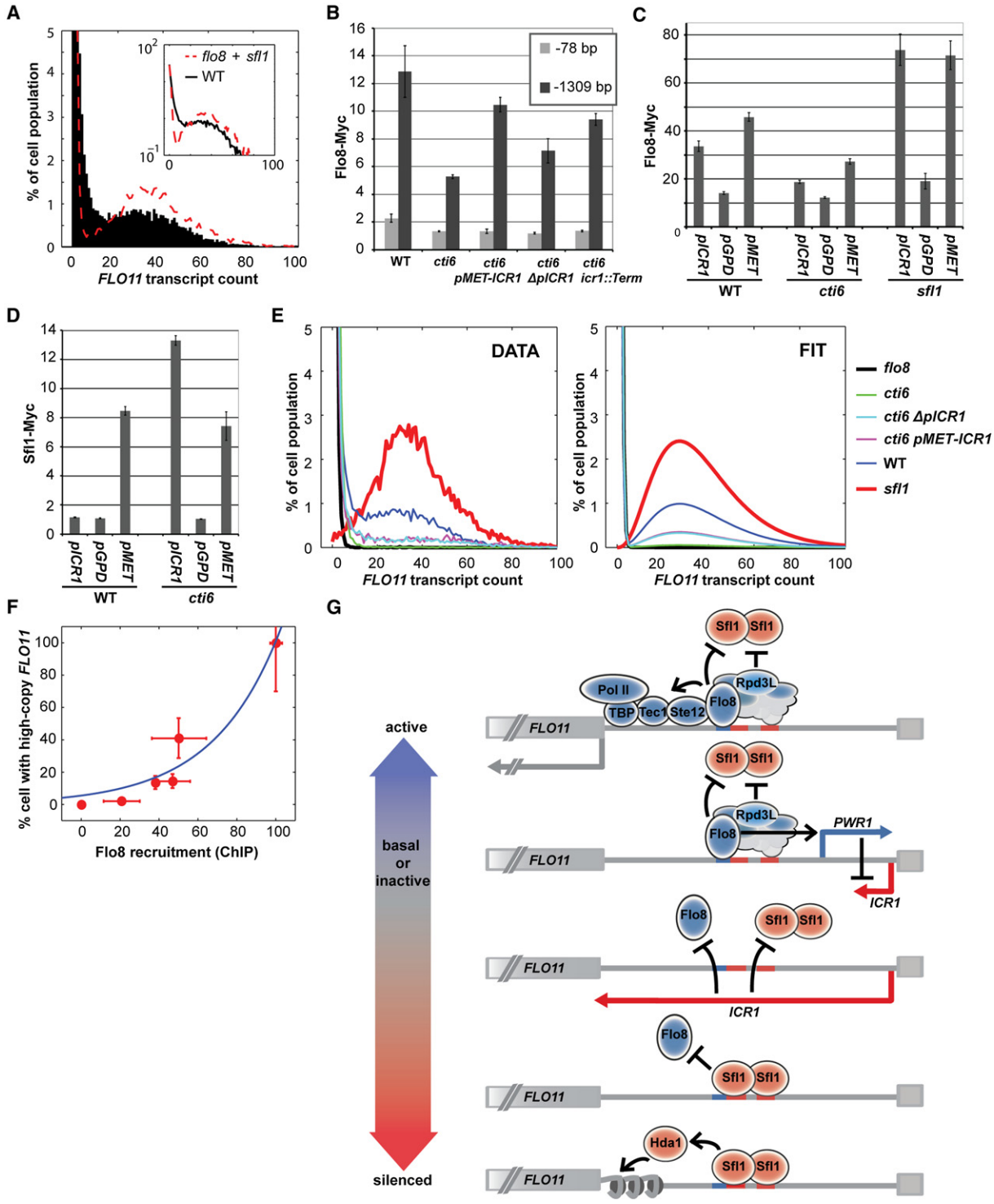

Figure 5. *ICR1* Regulates *FLO11* Expression by Interfering with Recruitment of Key Transcription Factors

(A) The distribution of *FLO11* detected in WT cells using RNA FISH (black bars in histogram; black line in inset logarithmic plot) can be recapitulated (red dashed lines) by combining the *FLO11* distributions observed in *flo8* and *sfl1* cell populations. The two mutant distributions were summed and weighted equally.

(B) Recruitment of myc-tagged Flo8 in haploid WT (yCW180), *cti6* (SBY1270), and *cti6* with reduced *ICR1* transcription (SBY1703, SBY1705, SBY1715), determined by ChIP followed by qPCR with primers specific to sites −78 bp (unbound control) and −1309 bp (binding region; Pan and Heitman, 2002) from the *FLO11* ATG. Data were normalized to unbound *ACT1* ORF and expressed as fold enrichment ±SEM.

Mechanistic Modeling of *FLO11* mRNA Distributions

Our approach assumed a simple mixture model of a Poisson and a gamma distribution (McLachlan and Peel, 2000). The Poisson distribution consists of one parameter, the normalized basal transcription rate $\lambda = 0.64$ mRNA. The gamma distribution consists of two parameters, the mean number of mRNA transcripts produced at each burst (i.e., average burst size; Raj et al., 2006), $\theta = 9.5$, and the normalized deactivation rate, $k = 3.9$. After the rates for these two distributions were determined, we fit the remaining *FLO11* mRNA distributions with the mixture model

$$p(mRNA, F, \lambda, k, \theta) = (1 - F) * \frac{\lambda^{mRNA}}{mRNA!} e^{-\lambda} + F * \frac{mRNA^{k-1} * e^{\frac{-mRNA}{\theta}}}{\theta^{k} * \Gamma(k)},$$

where F is the fraction of cells within a given population that exhibit high-copy (active) *FLO11* mRNA expression. The fit of the mixture model to the observed data was assessed using a maximum likelihood approach.

SUPPLEMENTAL INFORMATION

Supplemental Information includes three figures and Supplemental Experimental Procedures and can be found with this article online at doi:10.1016/j.molcel.2011.11.029.

ACKNOWLEDGMENTS

We thank Professors Rick Young (Whitehead Institute) and Joe Heitman (Duke University) for reagents to generate myc-tagged Sfl1; Chia Wu for strains yCW91 and yCW180; Leah Octavio for insightful comments on the manuscript; and Garrett Hauck, Lisa Nguyen, and Rafael Widjajahakim for help with media preparation and DNA isolation. This work was supported by National Institutes of Health grants GM035010 (G.R.F), GM40266 (G.R.F), and 1DP1OD003936 (A.v.O.); by National Science Foundation grant ECCS-0835623 (A.v.O.); and by the Deutsche Forschungs Gemeinschaft Forschungs Stipendium (G.N.). G.R.F. is an American Cancer Society Professor.

Received: August 9, 2011
Revised: October 18, 2011
Accepted: November 23, 2011
Published online: January 19, 2012

REFERENCES

Acar, M., Mettetal, J.T., and van Oudenaarden, A. (2008). Stochastic switching as a survival strategy in fluctuating environments. Nat. Genet. *40*, 471–475.

Batada, N.N., and Hurst, L.D. (2007). Evolution of chromosome organization driven by selection for reduced gene expression noise. Nat. Genet. *39*, 945–949.

Bertone, P., Stolc, V., Royce, T.E., Rozowsky, J.S., Urban, A.E., Zhu, X., Rinn, J.L., Tongprasit, W., Samanta, M., Weissman, S., et al. (2004). Global identification of human transcribed sequences with genome tiling arrays. Science *306*, 2242–2246.

Bumgarner, S.L., Dowell, R.D., Grisafi, P., Gifford, D.K., and Fink, G.R. (2009). Toggle involving cis-interfering noncoding RNAs controls variegated gene expression in yeast. Proc. Natl. Acad. Sci. USA *106*, 18321–18326.

Büttner, S., Eisenberg, T., Herker, E., Carmona-Gutierrez, D., Kroemer, G., and Madeo, F. (2006). Why yeast cells can undergo apoptosis: death in times of peace, love, and war. J. Cell Biol. *175*, 521–525.

Conlan, R.S., and Tzamarias, D. (2001). Sfl1 functions via the co-repressor Ssn6-Tup1 and the cAMP-dependent protein kinase Tpk2. J. Mol. Biol. *309*, 1007–1015.

David, L., Huber, W., Granovskaia, M., Toedling, J., Palm, C.J., Bofkin, L., Jones, T., Davis, R.W., and Steinmetz, L.M. (2006). A high-resolution map of transcription in the yeast genome. Proc. Natl. Acad. Sci. USA *103*, 5320–5325.

Davis, C.A., and Ares, M., Jr. (2006). Accumulation of unstable promoter-associated transcripts upon loss of the nuclear exosome subunit Rrp6p in *Saccharomyces cerevisiae*. Proc. Natl. Acad. Sci. USA *103*, 3262–3267.

FANTOM Consortium. (2005). The transcriptional landscape of the Mamm. genome. Science *309*, 1559–1563.

Femino, A.M., Fay, F.S., Fogarty, K., and Singer, R.H. (1998). Visualization of single RNA transcripts *in situ*. Science *28*, 585–590.

Güldener, U., Heck, S., Fiedler, T., Beinhauer, J., and Hegemann, J.H. (1996). A new efficient gene disruption cassette for repeated use in budding yeast. Nucleic Acids Res. *24*, 2519–2524.

Guo, B., Styles, C.A., Feng, Q., and Fink, G.R. (2000). A *Saccharomyces* gene family involved in invasive growth, cell-cell adhesion, and mating. Proc. Natl. Acad. Sci. USA *97*, 12158–12163.

Guthrie, C., and Fink, G.R. (2002). Guide to yeast genetics and molecular and cell biology. Methods Enzymol. *Vol. 350–351*.

Guttman, M., Amit, I., Garber, M., French, C., Lin, M.F., Feldser, D., Huarte, M., Zuk, O., Carey, B.W., Cassady, J.P., et al. (2009). Chromatin signature reveals over a thousand highly conserved large noncoding RNAs in mammals. Nature *458*, 223–227.

(C and D) ChIP followed by qPCR to measure recruitment to site −1309 bp from *FLO11* ATG of (C) myc-tagged Flo8 (in yCW180, SBY1723, SBY1720, SBY1270, SBY1717, SBY1703, SBY1324, SBY1729, and SBY1726) and (D) myc-tagged Sfl1 (in SBY1732, SBY1750, SBY1748, SBY1734, SBY1745, and SBY1737) in strains carrying either unmodified *pICR1* or indicated heterologous promoter controlling *ICR1*. Data were normalized to unbound *ACT1* ORF and given as fold enrichment ±SEM. The Sfl1-Myc allele may be hypomorphic, as recruitment detected with this allele is lower than expected in WT cells.
(E) Best fit of a Poisson distribution (black line) to the *FLO11* distribution observed in *flo8* cells (Flo8 recruitment to *FLO11* promoter = 0). Best fit of a gamma distribution (red line) to the *FLO11* distribution observed in *sfl1* cells (maximum Flo8 recruitment to *FLO11* promoter). Other curves (see legend) show fits of a mixture model that uses the Poisson and gamma distributions as parameters to set lower and upper bounds for Flo8 enrichment. The single free parameter in this mixture model is the fraction of cells exhibiting active (>5 dots) *FLO11* expression.
(F) A positive correlation exists between the amount of Flo8 recruitment measured by ChIP (B–D) and the fraction of cells exhibiting active *FLO11* expression. The best fit between the percentage of cells exhibiting active *FLO11* (empirical data in red measured by RNA FISH; error bars give SD) and Flo8 recruitment (empirical data in red measured by ChIP; error bars give SD) is indicated by the blue line.
(G) A comprehensive model to explain transcriptional variegation at the *FLO11* locus (Liu et al., 1996; Rupp et al., 1999; Guo et al., 2000; Conlan and Tzamarias, 2001; Pan and Heitman, 2002; Halme et al., 2004; Bumgarner et al., 2009; Octavio et al., 2009). Competition for binding between Sfl1 and Flo8 at respective sites on the *FLO11* promoter is at the heart of a toggle that controls *FLO11* transcription. Competitive binding contributes either to (1) a switch to the active state via Flo8-mediated recruitment of promoting factors or (2) a switch to the silenced state via Sfl1-mediated recruitment of silencing factors such as the Hda1 HDAC. Competition between Sfl1 and Flo8, influenced by Rpd3L HDAC activity, determines the ncRNA transcription program. Recruitment of Flo8 causes a pulse of *PWR1* transcription that promotes an active *FLO11* transcriptional state by interfering in *cis* with *ICR1* transcription. Flo8 binding also facilitates recruitment of additional *trans*-activators that stabilize the active state. Sfl1 binding recruits silencing factors, thereby promoting a reversible switch to a chromatin-mediated silenced *FLO11* promoter state. *ICR1* represses *FLO11* expression by occluding or ejecting *trans*-acting factors, such as Flo8 and Sfl1, from the *FLO11* promoter. Transcriptional progression of *ICR1* may "reset" the *FLO11* promoter to a basal state, so that Flo8 or Sfl1 may compete anew for binding. Thus, the ncRNAs influence the probability of the occurrence of downstream binding events that lead to active or silenced *FLO11* expression.

Halme, A., Bumgarner, S., Styles, C., and Fink, G.R. (2004). Genetic and epigenetic regulation of the *FLO* gene family generates cell-surface variation in yeast. Cell *116*, 405–415.

Huarte, M., Guttman, M., Feldser, D., Garber, M., Koziol, M.J., Kenzelmann-Broz, D., Khalil, A.M., Zuk, O., Amit, I., Rabani, M., et al. (2010). A large intergenic noncoding RNA induced by p53 mediates global gene repression in the p53 response. Cell *142*, 409–419.

Janke, C., Magiera, M.M., Rathfelder, N., Taxis, C., Reber, S., Maekawa, H., Moreno-Borchart, A., Doenges, G., Schwob, E., Schiebel, E., and Knop, M. (2004). A versatile toolbox for PCR-based tagging of yeast genes: new fluorescent proteins, more markers and promoter substitution cassettes. Yeast *21*, 947–962.

Kaern, M., Elston, T.C., Blake, W.J., and Collins, J.J. (2005). Stochasticity in gene expression: from theories to phenotypes. Nat. Rev. Genet. *6*, 451–464.

Lee, T.I., Johnstone, S.E., and Young, R.A. (2006). Chromatin immunoprecipitation and microarray-based analysis of protein location. Nat. Protoc. *1*, 729–748.

Lehner, B. (2008). Selection to minimise noise in living systems and its implications for the evolution of gene expression. Mol. Syst. Biol. *4*, 170.

Li, B., Carey, M., and Workman, J.L. (2007). The role of chromatin during transcription. Cell *128*, 707–719.

Liu, H., Styles, C.A., and Fink, G.R. (1996). *Saccharomyces cerevisiae* S288C has a mutation in *FLO8*, a gene required for filamentous growth. Genetics *144*, 967–978.

Lu, J., and Tsourkas, A. (2009). Imaging individual microRNAs in single mammalian cells *in situ*. Nucleic Acids Res. *37*, e100. 10.1093/nar/gkp482.

Martens, J.A., Laprade, L., and Winston, F. (2004). Intergenic transcription is required to repress the *Saccharomyces cerevisiae SER3* gene. Nature *429*, 571–574.

McLachlan, G.J., and Peel, D. (2000). Finite Mixture Models (New York: John Wiley and Sons).

Neil, H., Malabat, C., d'Aubenton-Carafa, Y., Xu, Z., Steinmetz, L.M., and Jacquier, A. (2009). Widespread bidirectional promoters are the major source of cryptic transcripts in yeast. Nature *457*, 1038–1042.

Octavio, L.M., Gedeon, K., and Maheshri, N. (2009). Epigenetic and conventional regulation is distributed among activators of *FLO11* allowing tuning of population-level heterogeneity in its expression. PLoS Genet. *5*, e1000673. 10.1371/journal.pgen.1000673.

Pan, X., and Heitman, J. (2002). Protein kinase A operates a molecular switch that governs yeast pseudohyphal differentiation. Mol. Cell. Biol. *22*, 3981–3993.

Pena, J.T., Sohn-Lee, C., Rouhanifard, S.H., Ludwig, J., Hafner, M., Mihailovic, A., Lim, C., Holoch, D., Berninger, P., Zavolan, M., and Tuschl, T. (2009). miRNA in situ hybridization in formaldehyde and EDC-fixed tissues. Nat. Methods *6*, 139–141.

Raj, A., and van Oudenaarden, A. (2008). Nature, nurture, or chance: stochastic gene expression and its consequences. Cell *135*, 216–226.

Raj, A., Peskin, C.S., Tranchina, D., Vargas, D.Y., and Tyagi, S. (2006). Stochastic mRNA synthesis in mammalian cells. PLoS Biol. *4*, e309. 10.1371/journal.pbio.0040309.

Raj, A., van den Bogaard, P., Rifkin, S.A., van Oudenaarden, A., and Tyagi, S. (2008). Imaging individual mRNA molecules using multiple singly labeled probes. Nat. Methods *5*, 877–879.

Roberts, R.L., and Fink, G.R. (1994). Elements of a single MAP kinase cascade in *Saccharomyces cerevisiae* mediate two developmental programs in the same cell type: mating and invasive growth. Genes Dev. *8*, 2974–2985.

Rupp, S., Summers, E., Lo, H.J., Madhani, H., and Fink, G. (1999). MAP kinase and cAMP filamentation signaling pathways converge on the unusually large promoter of the yeast *FLO11* gene. EMBO J. *18*, 1257–1269.

Sambrook, J., Fritsch, E.F., and Maniatis, T. (1989). Molecular Cloning: A Laboratory Manual, Second Edition (Plainview, NY: Cold Spring Harbor Lab Press).

Seila, A.C., Calabrese, J.M., Levine, S.S., Yeo, G.W., Rahl, P.B., Flynn, R.A., Young, R.A., and Sharp, P.A. (2008). Divergent transcription from active promoters. Science *322*, 1849–1851.

van Dijk, E.L., Chen, C.L., d'Aubenton-Carafa, Y., Gourvennec, S., Kwapisz, M., Roche, V., Bertrand, C., Silvain, M., Legoix-Né, P., Loeillet, S., et al. (2011). XUTs are a class of Xrn1-sensitive antisense regulatory non-coding RNA in yeast. Nature *475*, 114–117.

Vermaak, D., Ahmad, K., and Henikoff, S. (2003). Maintenance of chromatin states: an open-and-shut case. Curr. Opin. Cell Biol. *15*, 266–274.

Xu, Z., Wei, W., Gagneur, J., Perocchi, F., Clauder-Münster, S., Camblong, J., Guffanti, E., Stutz, F., Huber, W., and Steinmetz, L.M. (2009). Bidirectional promoters generate pervasive transcription in yeast. Nature *457*, 1033–1037.

Zenklusen, D., Larson, D.R., and Singer, R.H. (2008). Single-RNA counting reveals alternative modes of gene expression in yeast. Nat. Struct. Mol. Biol. *15*, 1263–1271.